125
6-6-80

AR. 1277

ornl

MASTER

ORNL/TM-7239

OAK
RIDGE
NATIONAL
LABORATORY

UNION
CARBIDE

High-Resolution Spectral Analysis of Light from Neutral Beams and Ion Source Plasmas

D. H. McNeill
J. Kim

OPERATED BY
UNION CARBIDE CORPORATION
FOR THE UNITED STATES
DEPARTMENT OF ENERGY

ORNL/TM-7259
Dist. Category UC-20a

Contract No. W-7405-eng-26

FUSION ENERGY DIVISION

HIGH-RESOLUTION SPECTRAL ANALYSIS OF LIGHT FROM NEUTRAL BEAMS AND ION SOURCE PLASMAS

D. H. McNeill
Princeton Plasma Physics Laboratory

J. Kim

Date Published: May 1980

NOTICE **This document contains information of a preliminary nature. It is subject to revision or correction and therefore does not represent a final report.**

Prepared by the
OAK RIDGE NATIONAL LABORATORY
Oak Ridge, Tennessee 37830
operated by
UNION CARBIDE CORPORATION
for the
DEPARTMENT OF ENERGY

CONTENTS

ABSTRACT

The spectral distributions of Balmer alpha emission from 7- and 22-cm-diam neutral hydrogen beams have been measured with a Fabry-Perot interferometer to obtain information on the beam energy, divergence, and species composition. Results of these measurements are compared with other data on the beam properties to evaluate high-resolution spectroscopy as a beam diagnostic technique. Measurements on ion source plasmas and on beam-produced background plasmas yield average neutral atom energies of approximately 0.3 and 2.5 eV, respectively.

1. INTRODUCTION

Indirect monitoring of the divergence, species composition, and energy of neutral beams is desirable in injection heating experiments because the interaction between a plasma and a neutral beam is sensitive to the beam properties. Knowledge of these properties is particularly important for evaluating the efficiency of energy transfer from the beam to the plasma. Spectroscopic techniques have great potential as passive diagnostics of beam quality. Techniques that have already been employed include use of grating spectrographs with an optical multichannel analyzer,[1] a rapid-scan mirror,[2] and a light guide array.[3] Here we present some preliminary data, obtained by means of a Fabry-Perot interferometer (FPI), on the Doppler-modified profiles of hydrogen Balmer alpha (H_α) emission from neutral hydrogen beams and injector ion sources, and we discuss the use of this technique as a beam diagnostic. Our data yielded information on the mechanism that produces excited hydrogen atoms in the ion source plasmas and on the angular distribution and energy spectrum of the energetic beam atoms.

The advantages of the FPI are its high resolution, its rapid linear scan (several orders in a 20-ms scan), and its high light-gathering power. High resolution makes it possible to measure accurately the profile of the H_α light emitted by the ion sources and beams. We thus were able to view the beam light at angles nearly 90° to the beam axis and thereby to avoid distortion of the spectral profiles from geometric effects or longitudinal variations in the beam properties and background gas density. The rapid linear scan makes it possible to examine the time variation of the ion source discharge or beam characteristics.

We begin with a discussion of the physical processes and methods involved in the experiments: the Doppler effect, the operation of the FPI and the interpretation of data obtained through its use, the broadening of line emission from the ion source plasmas, and the spectroscopic measurement of neutral beam characteristics. Data are presented from experiments on ion sources, on 7-cm-diam hydrogen beams, and on high-power, 22-cm-diam neutral hydrogen beams. The data from the neutral beam experiments are compared with other information on the properties

of interest to demonstrate that the technique worked well under certain conditions. The possibilities of and limitations on the further use of this method are discussed in the light of our present experience and the diagnostic needs of fusion experiments.

2. EXPERIMENTAL TECHNIQUE

2.1 DOPPLER EFFECT

The light from an emitting atom that is moving relative to an observer will appear to be shifted in wavelength. This effect is known as the Doppler shift. In our case the emitting atom is a hydrogen atom in the n = 3 state undergoing a transition to the n = 2 state to produce a Balmer alpha (H_α) photon with a proper wavelength of 6563 Å. The shifted wavelength resulting from the Doppler effect is given by

$$\lambda = \lambda_o \frac{1 - (v/c) \cos \theta}{[1 - (v^2/c^2)]^{1/2}} , \qquad (1)$$

where θ is the angle between the velocity $\bar{v}$ of the emitting atom and the observation vector $\hat{k}$ from the atom to the observer, c is the speed of light, and λ_o is the proper (unshifted) wavelength (Fig. 1). The denominator in this expression gives the transverse (relativistic) Doppler effect, which is negligible at low velocities. For perfect collimation of the viewing system (i.e., $\hat{k}$ in one direction only) and $\bar{v}$ uniform (i.e., the same magnitude and direction of $\bar{v}$ for each of a group of emitters), the Doppler shift changes monochromatic light from the source atoms into monochromatic light at a different wavelength.

If the direction or magnitude of $\bar{v}$ varies among a group of emitting particles or the optical collimation is not perfect, then the initial source wavelength is shifted into different wavelengths. For a large number of emitters, the light is effectively spread out to produce what is known as a Doppler-broadened profile. Nonuniformity of $\bar{v}$ may be due to a spread in the magnitude (e.g., a Maxwellian distribution in a thermal gas) or in the direction of the velocity vectors of the emitting particles (e.g., the isotropic distribution of a thermal gas or the finite divergence of a beam). Imperfect collimation is a characteristic of the experimental apparatus, resulting in particular from a finite angle of acceptance of light from the source, such as would occur with a finite detector aperture at the focus of a collimating lens in the

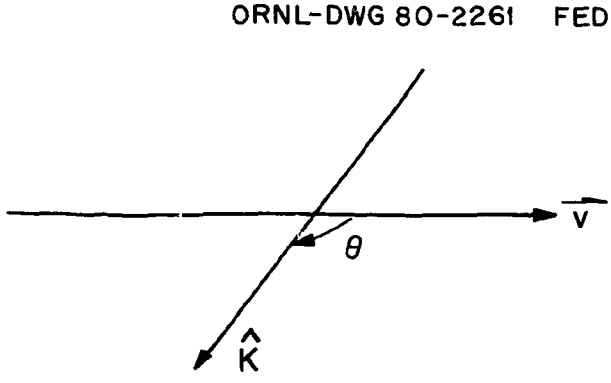

Fig. 1. The Doppler effect.

detection system and from instrument effects, such as finite resolution. We are interested in the distribution of $\bar{v}$ in two cases: (1) injector ion source plasmas and beam-generated background plasmas and (2) neutral beams. In the first case, the distribution in magnitude is of interest because we assume isotropy, and in the second, the distribution in direction is of interest because we assume that the beam particles are monoenergetic or at least bunched in discrete monoenergetic groups.

2.2 FABRY-PEROT INTERFEROMETER

A Fabry-Perot interferometer consists of two partially transmitting flat mirrors mounted parallel to one another (Fig. 2). The instrument used in these experiments was a Burleigh Instruments RC-10 piezoelectric scanning FPI. When the FPI cavity is illuminated at one end by a beam of collimated monochromatic light, it will transmit the light if the optical distance between the surfaces is an integral number of half wavelengths. This condition is equivalent to the occurrence of constructive interference when the relationship $2d \cos \phi = m\lambda$ is satisfied. Here, d is the distance between the mirrors (the medium between the mirrors is assumed to have a refractive index of unity), ϕ is the angle between the normal to the mirrors and the incident beam, m (an integer) is the order of interference, and λ is the wavelength. As m goes through consecutive integral values (m is varied by changing d, since ϕ is fixed at 90°), we obtain a repetitive output or fringes. (For a more detailed discussion of the FPI see, for example, Born and Wolf's *Principles of Optics*.[4])

The range of wavelengths that can be seen through the interferometer in the same order without overlapping into other orders is called the free spectral range (FSR) and is given by

$$\Delta\lambda_{FSR} = \frac{\lambda^2}{2d}, \tag{2}$$

with all dimensions in the same units. Figure 3 shows the response to a monochromatic light source of a scanning FPI with collimating optics and

detector arranged as shown in Fig. 2. The smallest attainable width (FWHM) of the peaks is called the minimum resolving band width $\Delta\lambda_R$. The instrument function of an FPI is characterized by the finesse (F), which is defined by

$$F = \frac{\Delta\lambda_{FSR}}{\Delta\lambda_R} . \tag{3}$$

The finesse is determined by numerous factors, including the reflectivity, flatness, and parallelism of the mirrors; the focal length and aperture of the collimator; and mechanical vibrations. The inverse square of the overall finesse is given by the sum of the inverse squares of the finesse owing to each of these factors. In our experiments, the actual finesse was measured by using a helium-neon (He-Ne) laser as a narrow line-width source. The laser output consisted of from one to four lines, each with a line width of about 0.001 Å, roughly 0.007 Å apart, for a net laser line width of 0.02 Å or less. The finesse was optimized by adjusting the mirror parallelism to obtain maximum transmission of the laser beam. In practice, F = 40-80, with a typical operating value of 60.

In the arrangement shown in Fig. 2, the plate separation can be periodically varied by means of the piezoelectric drive. The collimating lens and pinhole collect light within a specific solid angle. For a single wavelength input, the photomultiplier output will have the appearance of Fig. 3a, with successive peaks attributable to transmission at different plate separations. The number of peaks is determined by the amplitude of the ramp voltage (i.e., the total change in d). The piezoelectric drive is activated by a sawtooth ramp voltage (rise time of 20 ms to 1000 s) having a 15-ms retrace, during which the entire FPI pattern is repeated in reverse. For a source that is slightly broadened (but much less than the FSR), the output spikes will be wider, whereas if several wavelengths are present simultaneously, there will be multiple peaks corresponding to each wavelength in every order (see Fig. 3b). If the separation between these wavelengths exceeds the FSR, then the neighboring peaks may correspond to different interference orders. The

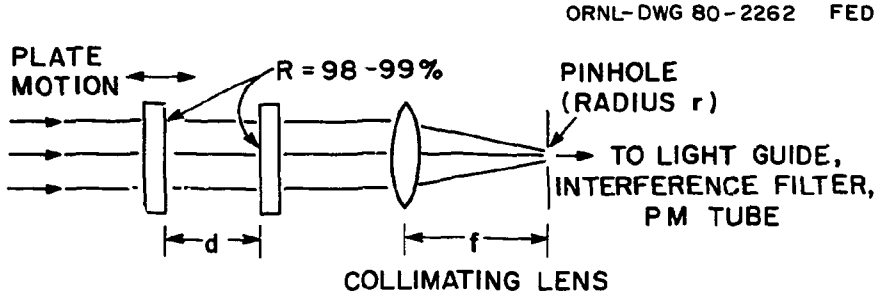

Fig. 2. Optical layout of a Fabry-Perot interferometer and associated collimating optics and detector.

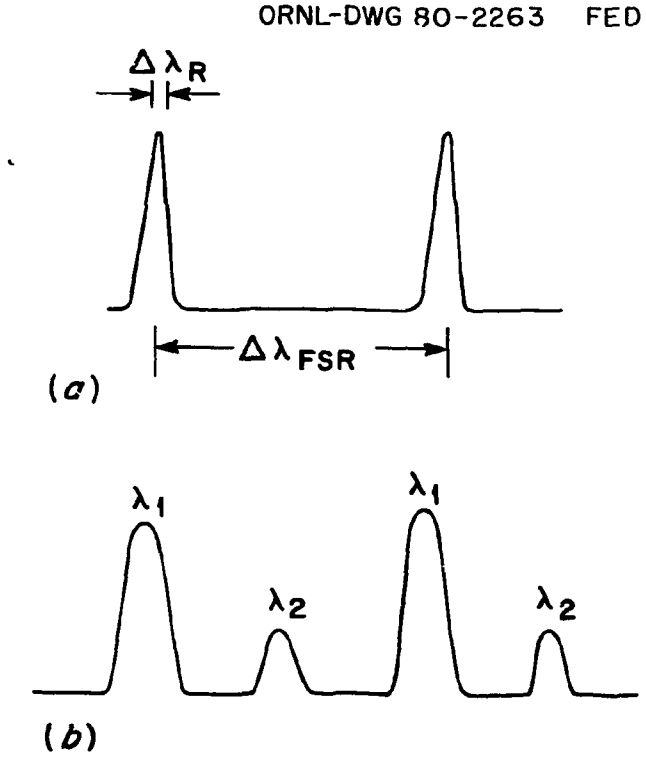

Fig. 3. Output traces from a Fabry-Perot interferometer for (a) a single, narrow-band light source, illustrating the resolution bandwidth and free spectral range (instrument response), and (b) a multiple wavelength, broadened source.

wavelength separation can be evaluated using the relation: for known λ_2 and unknown λ_1, both visible in an FPI trace, $\lambda_1 = \lambda_2 + \Delta\lambda + n\Delta\lambda_{FSR}$, where $\Delta\lambda(<\Delta\lambda_{FSR})$ is the apparent separation between the two wavelengths on the FPI trace and n is an integer or zero. The value of λ_1 must be approximately known to obtain the proper value of n.

2.3 LINE BROADENING IN PLASMAS

In the ion source plasmas, the H_α spectrum line undergoes (1) the natural broadening intrinsic to atomic transitions and the lifetime of states (about 10^{-4} Å); (2) the collisional Stark broadening resulting from the electric microfield of the plasma (about 0.02 Å); (3) Zeeman splitting, attributable to the magnetic field in the source (less than 0.01 Å); (4) the fine structure splitting of H_α (it is sufficient for our purposes to regard the H_α line as made up of two components separated by 0.14 Å); and (5) Doppler broadening.[5] [For atoms with temperature T_o(eV), the full-width half-maximum (FWHM) of the Doppler-broadened line at 6563 Å is $\Delta\lambda_{1/2}$ (Å) = 0.504 $T_o^{1/2}$. A nonthermal distribution yields a profile whose width depends on the distribution function.] Doppler broadening is, by far, the largest contribution to the width of the H_α line from the ion sources. The apparent broadening owing to instrument width can be determined from the finesse measurements of the previous section.

2.4 BEAM DIAGNOSTICS

The H_α light produced by neutral beams comes both from the high-energy atoms in the beam and from the low-energy atoms in the background beam plasma, produced by the beam as it passes through the residual hydrogen gas. Interpreting the H_α spectrum produced by neutral beams is, therefore, more complex than interpreting that of an isotropic stationary plasma. Viewed perpendicular to the beam axis, the H_α spectrum consists of overlapping contributions from the two sources. Since the atoms in the beam plasma are at least approximately isotropically distributed in the laboratory frame, their line emission is not

shifted, but only broadened, as in a stationary plasma. The two contributions can be separated in wavelength by viewing the beam at an off-90° angle to its axis, because then the beam light is Doppler shifted. The concept of the spectroscopic beam diagnostics is illustrated in Fig. 4, where v_b is the beam particle speed, $\hat{k}$ is the observation direction, $\theta = 90° + \theta'$ is the viewing angle, and α is the angle between the velocity of a given particle and the axis of the beam. We shall neglect the beam plasma component in deriving the H_α profile of the beam light.

We first consider a view perpendicular to the beam axis ($\theta = 90°$). Let us assume that the optical system has perfect collimation and resolution and, for mathematical convenience, that the beam has a Gaussian angular distribution $B(\alpha) = B_o \exp(-4\alpha^2/\alpha_e^2)$, where α_e is the full-width 1/e divergence angle of the beam. In terms of the FWHM angle of the beam (α_o), which is often measured experimentally, the distribution becomes $B(\alpha) = B_o \exp(-4 \ln 2\alpha^2/\alpha_o^2)$. We shall refer to α_o as the angular divergence of the beam. This notion of divergence can be extended easily to non-Gaussian beams.

The transverse Doppler shift causes a uniform displacement of all light from the beam particles at speed v_b and can be neglected in calculating the shape of the Doppler profile of the beam light. The Doppler shift for a beam atom with angle α viewed perpendicular to the beam direction ($\theta = 90°$) is found from Eq. (1) to be

$$\Delta\lambda \equiv \lambda - \lambda_o = \frac{v_b \lambda_o}{c} \sin\alpha \doteq \frac{v_b \lambda_o \alpha}{c} ,$$

where λ_o is the unshifted wavelength of H_α and α is assumed to be small so that $\sin\alpha \doteq \alpha$. Hence

$$\alpha \doteq \frac{c\Delta\lambda}{v_b \lambda_o} .$$

The combined emission from the beam particles at all angles α appears as a broadened spectrum corresponding to the angular distribution of the

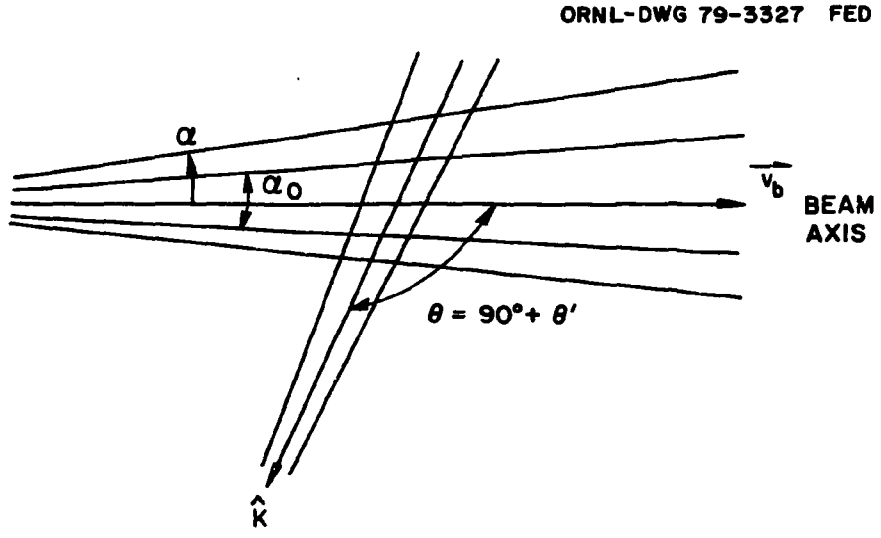

Fig. 4. The geometry for the measurements on neutral beams.

beam atoms. The angular distribution $B(\alpha)$ and the spectral distribution $S(\lambda)$ of the light from the beam are related by $B(\alpha)\, d\alpha = S(\lambda)\, d\lambda$. Thus, the spectral distribution of the beam light is

$$S(\lambda) = S_o \exp\left(-\frac{4\ \ell n\ 2\Delta\lambda^2}{\Delta\lambda_o^2}\right), \tag{4}$$

where $\Delta\lambda_o \equiv v_b\lambda_o\alpha_o/c$ is the FWHM of the spectral distribution for a beam viewed at 90°. The corresponding beam divergence thus is

$$\alpha_o = 3.3E_b^{-1/2}\Delta\lambda_o\ , \tag{5}$$

where E_b is the beam energy (accelerating voltage) in eV, α_o is in radians, and $\Delta\lambda_o$ is in Å. The spreading of the H_α line is due to the small component of the beam atom velocity along the line of sight ($\hat{k}$) in Fig. 4, but the center of the profile is unshifted (except for the transverse Doppler effect at high energies). Non-Gaussian profiles will yield spectral profiles that differ in shape from Eq. (4) but that are related to the beam angular distribution in a similar way.

Viewing the beam at an "off-perpendicular" angle ($\vartheta \neq 90°$) not only separates the H_α spectra of the beam and beam plasma light, but yields information on the speed of the beam atoms and can reveal the existence of groups of beam atoms with energies less than the accelerating voltage. For views at angles that are slightly off perpendicular (small θ') (Fig. 4) and for small divergence angles (α), a derivation similar to that of Eq. (4) gives

$$S(\lambda) = \frac{\text{const}}{\cos\theta'} \exp\left\{-\frac{[\lambda - \lambda_o(1 + \frac{v_b}{c}\sin\theta')]^2}{\Delta\lambda_o^2}\ 4\ \ell n\ 2\right\}\ , \tag{6}$$

which corresponds to a Gaussian distribution with FWHM

$$\Delta\lambda_o \equiv \frac{v_b \lambda_o \alpha_o}{c} \cos \theta'$$

centered at

$$\lambda_o\left(1 + \frac{v_b}{c} \sin \theta'\right),$$

for a shift of the line center by

$$\frac{\lambda_o v_b}{c} \sin \theta' .$$

For $\theta' \ll 1$, the broadening is the same as that in Eq. (4). For large angles off perpendicular (or, by extension, for large divergence angles), however, the observed H_α profiles become substantially different from Eq. (6). (See Appendix A for a discussion of these changes in the profile.) Hence, there was a need to see if the spectrum could be analyzed at small θ'. (Experiments conducted by Burrell et al.,[1] Ulrickson and Bussac,[2] and Bonnal et al.[3] employed large θ'; the latter two also did not consider line shape.) Because of the small wavelength intervals involved, a high-resolution instrument was necessary. Other problems associated with beam optics and the interpretation of spectral data are discussed briefly in Appendix B.

3. DATA AND DISCUSSION

3.1 ION SOURCE EXPERIMENTS

We examined the H_α light from a 15-cm-diam picket-fence line-cusp ion source[6] and a 7-cm-diam duoPIGatron ion source[7] to determine the energy of the neutral atoms in the discharge. As shown in Fig. 5, the measurements were made through a port 1.25 cm in diameter that viewed the discharge region roughly 5 cm from the plasma grid (first accelerator electrode). No measurements were made while a beam was being extracted. The system was aligned by passing a He-Ne laser beam through a viewing port opposite the observation port and backwards along the optical train. An interference filter (FWHM 10, 30, or 100 Å) was placed in the photomultiplier housing to block out background light from the filaments of the picket-fence line-cusp source. The photomultiplier output could be filtered by an RC filter to smooth the profiles, but unfiltered data were always taken during each run to ensure that the RC filter did not distort the profiles.

Figure 6 shows oscilloscope traces of data from a 7-cm duoPIGatron source. Figure 7 is a plot of the signal from the right-hand side of the expanded spike shown in Fig. 6b as a function of the square of the wavelength shift. The FWHM of the spike is about 0.26 Å. It is not necessarily true that the observed profile corresponds to a thermal distribution of the emitting source atoms. The measured and theoretical instrument profiles[4] are sufficiently wide to fill out the wings of a spectral profile obtained from the slow electron impact dissociation products of H_2, which do not have a thermal distribution.[8]

The ion source plasmas yielded a symmetric line profile with a FWHM of 0.26 ± 0.02 Å under all discharge conditions (arc current, arc voltage, and gas pressure) and at all times during the discharges. One exception was the plasma from a duoPIGatron source modified with a hot tungsten predissociator[9] for increasing the proton fraction in the discharge. In that case the profile was asymmetric, but was roughly as wide as in the other cases. The reason for this asymmetry is unclear at present. The

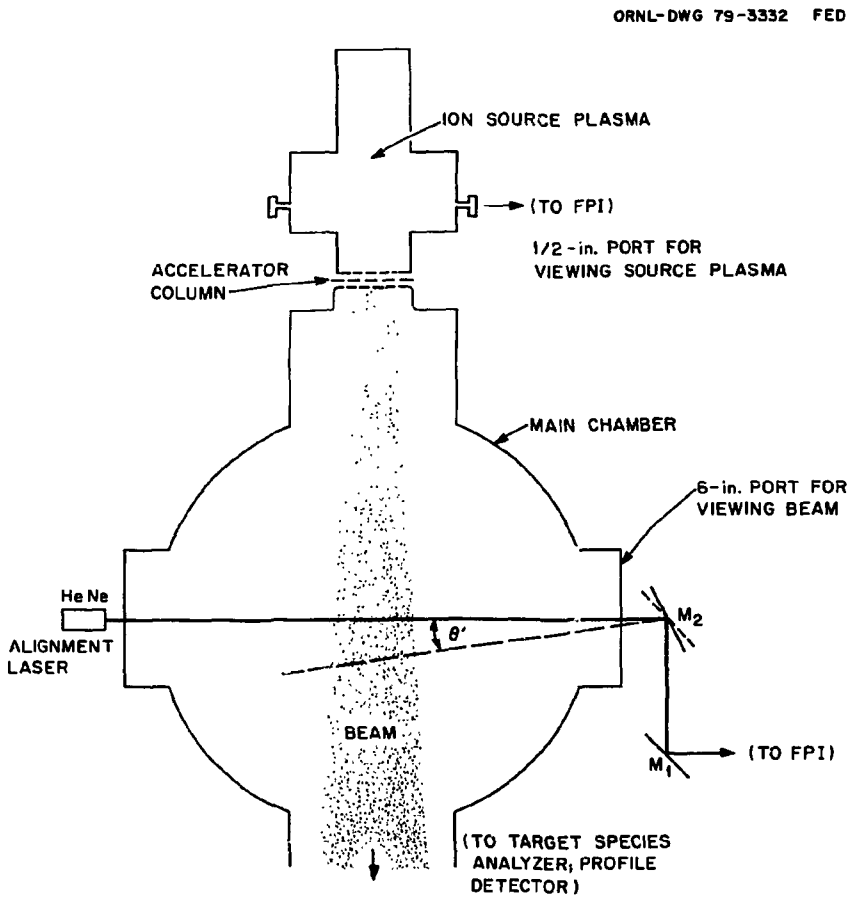

Fig. 5. The experimental arrangements for the measurements on 7-cm sources and beams.

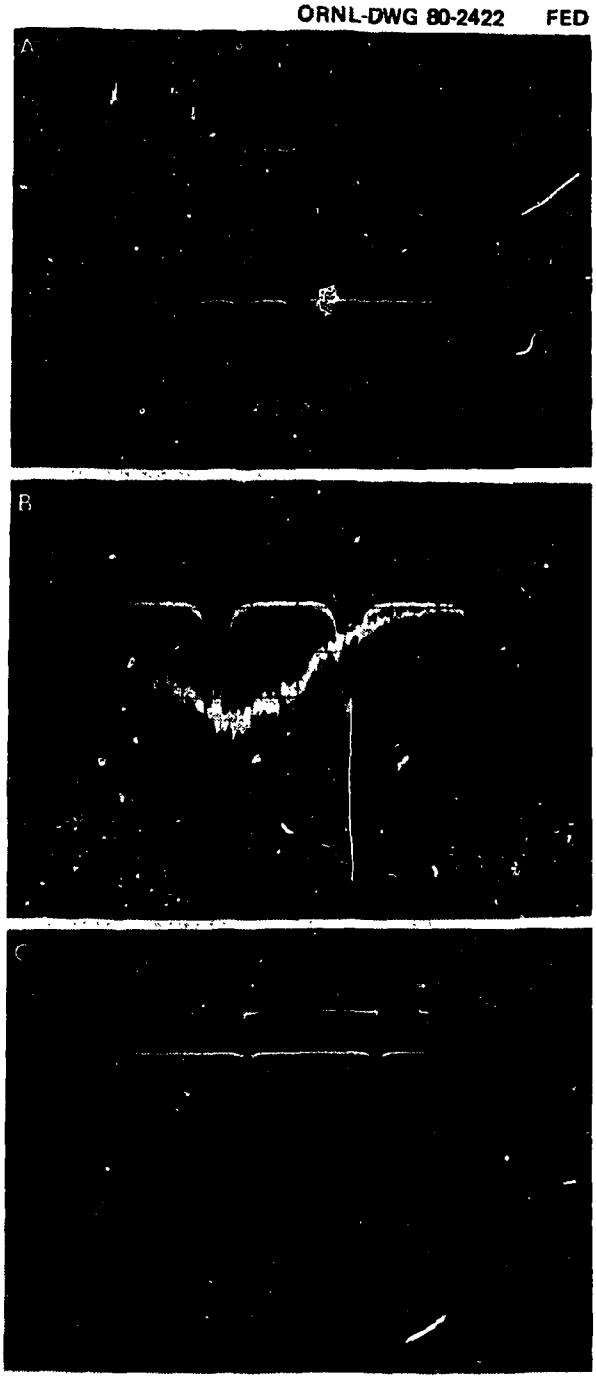

Fig. 6. Oscilloscope traces of data from a 7-cm duoPIGatron source: (a) the arc current and electrically unfiltered photomultiplier output (three orders during the 200-ms arc pulse); (b) the RC-filtered photomultiplier output triggered at the beginning of the arc, together with the trace of a single spike near the middle of the discharge magnified ten times; and (c) the response of the entire optical system to a He-Ne laser, together with the trace of a single spike magnified ten times. The short scribe mark in (c) corresponds to the FWHM of the 10x spike and the long scribe mark to the free spectral range of the interferometer at 6328 Å. This shows that the finesse $F \sim 60$.

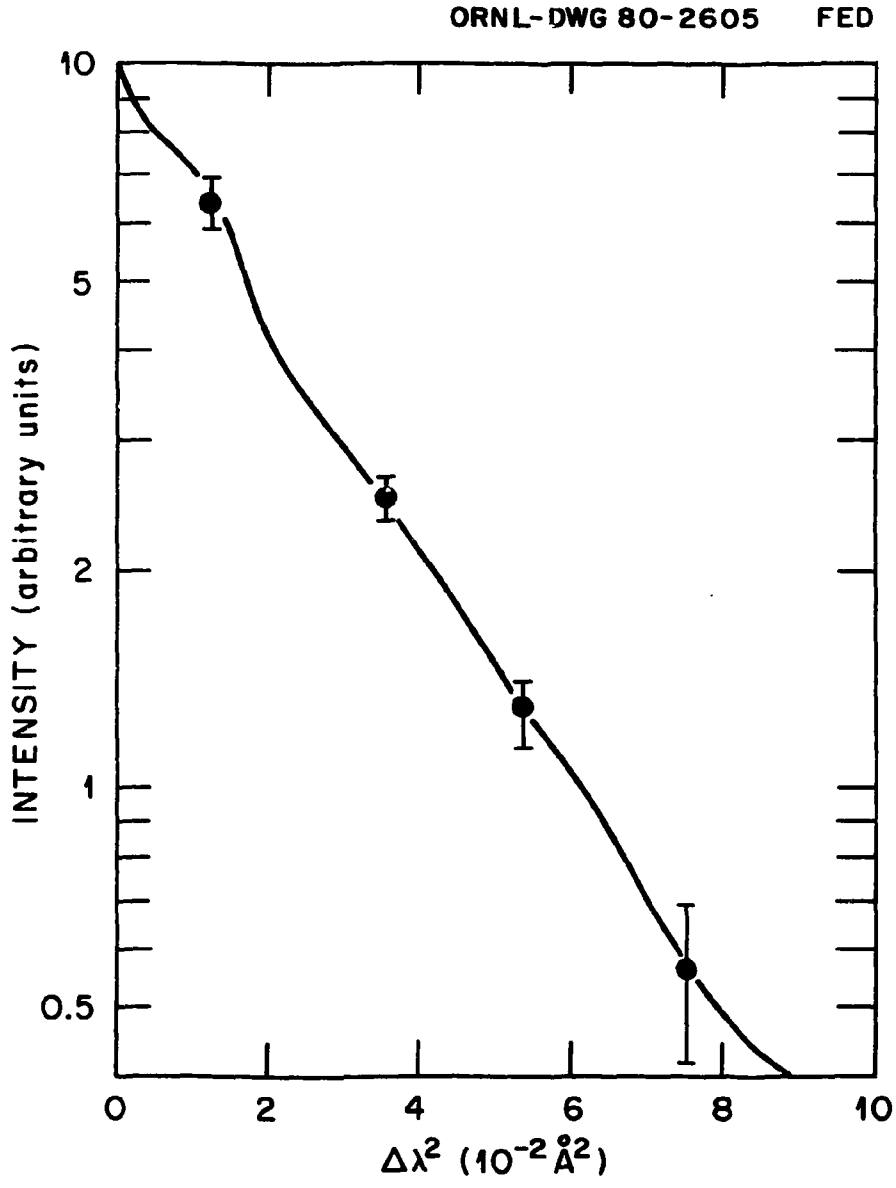

Fig. 7. A semilog plot of the fast-swept trace shown in Fig. 6b. The FWHM of this profile is about 0.26 Å.

observed line width corresponds to a characteristic (most probable) neutral atom energy of 0.27 ± 0.04 eV in the discharge.* This energy corresponds to the energy of the product atoms produced in dissociative excitation of H_2 molecules by low-energy electron impact.[8] The energy spectrum of these slow dissociation products is deficient in both high- and low-energy atoms, as compared with a thermal distribution having the same most probable energy. Relatively few of the fast dissociation atoms produced by electrons of energies above ∿28 eV (i.e., those atoms with energies of 2-4 eV) should appear in the H_α spectrum from these source plasmas ($n_e \sim 1\text{-}2 \times 10^{12}$ cm^{-3}, $T_e \sim 2\text{-}4$ eV).[6,7]

3.2 PERPENDICULAR VIEWS OF 7-cm BEAMS

The optical arrangement for viewing the beams extracted from a 7-cm-diam duoPIGatron source is shown in Fig. 5. The beam was viewed at 90° to the beam axis about 60 cm from the accelerating electrodes to test the feasibility of this technique for determining the beam divergence and other characteristics. Mirror M_2 could be rotated to view the beam at small angles off 90°. The parallelism of the FPI mirrors and the direction the optics were aimed with respect to the beam axis could be checked by using a He-Ne laser, as shown in the figure.

Because the viewing region in this case was still in the beam neutralization region and no bending magnets were used to remove charged particles, ions and neutrals of various molecules were present in addition to the neutral and ionized hydrogen atoms. We were, of course, only observing one species — hydrogen atoms in the n = 3 state, just as they emit an H_α photon. We stress here that the FPI *does not* see light from

---

*We note a change in the results reported by W. L. Stirling et al.[7] in that we no longer regard the neutral atoms as having a true kinetic temperature, as such, although the distribution is fairly close to Maxwellian. The characteristic energy is changed from 0.35 ± 0.07 eV to 0.27 ± 0.04 eV owing to a reanalysis of the data in the light of a correction to the FPI plate separation.

ions of any kind or from H_2, H_3, or higher molecules. All of these species may contribute to calorimetric signals or, in the case of the ions, to analyzing magnet signals, thereby yielding different results from the spectroscopic measurements. The hydrogen atoms that are seen may be from the beam itself or from the beam plasma.

Figure 8a shows the signals from 7-cm-diam, 0.5-A beams with accelerating voltages of 10 and 20 kV (left and right peaks, respectively) viewed at 90° to the beam axis. Figure 8b shows the data for a 20-kV, 0.5-A beam with two interference orders in the trace. The signal on the right-hand side of the left peak of Fig. 8b is plotted in Fig. 9 as a function of the square of the relative wavelength displacement from the center of the peak. This semilog plot reveals a narrow component with a FWHM of about 0.75 Å, implying that the beam plasma light is from atoms with energies of about 2.5 eV. The results of off-perpendicular views confirm that this narrow component is the beam plasma component. The semilog plot also reveals a broad component with a FWHM of about 2.5 Å, implying a beam FWHM divergence of roughly 3.4°. This spectroscopically determined divergence angle is in good agreement with the calorimetrically determined profile shape on a target, which yielded a divergence of 3.2°. We have assumed that there are only two components in this profile, or at least that the light in the broad component is mostly due to full-energy H atoms, and that both components have Gaussian shapes. The original data of Fig. 8b are fairly well reproduced by a model using these assumptions; however, the data are too noisy to check the distribution at large angles. A constant background light level in the data of Fig. 8b would cause our estimate of the fast component width, and thus the divergence, to be high (see Appendix C). Data taken with a larger free spectral range on the FPI and with different beam energies indicate that this background level is low in the 90° case.

3.3 OFF-PERPENDICULAR VIEWS OF 7-cm BEAMS

The beam could be viewed off 90° by rotating mirror M_2 of Fig. 5 and the viewing angle determined by measuring the deflection of the He-Ne alignment laser beam. Figure 10 shows traces of data taken from

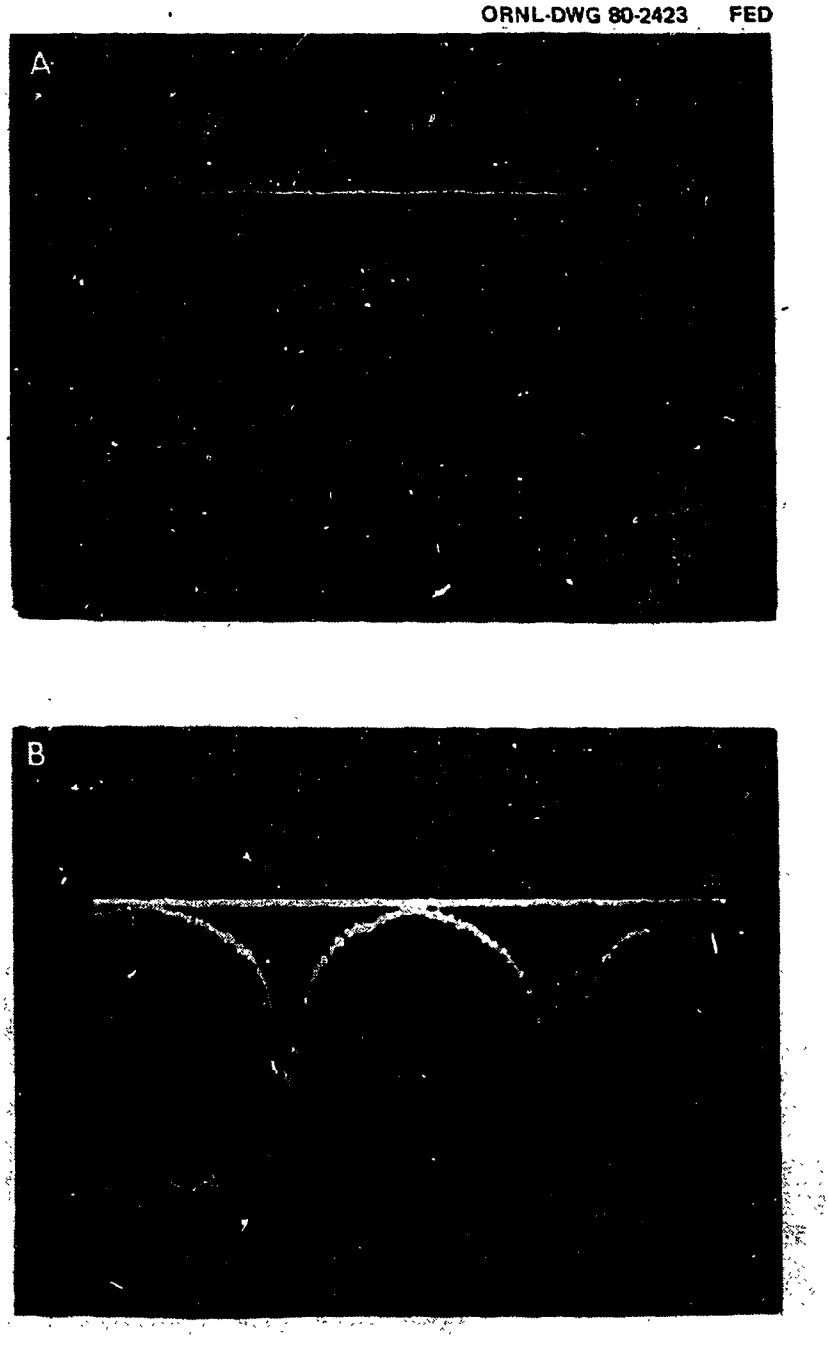

Fig. 8. Data from 90° views of 7-cm beams, including (a) the FPI response to 0.5-A beams with 10- and 20-kV accelerating voltages (left and right peaks, respectively) and (b) a similar sweep for a 20-kV 0.5-A beam, showing two orders of interference.

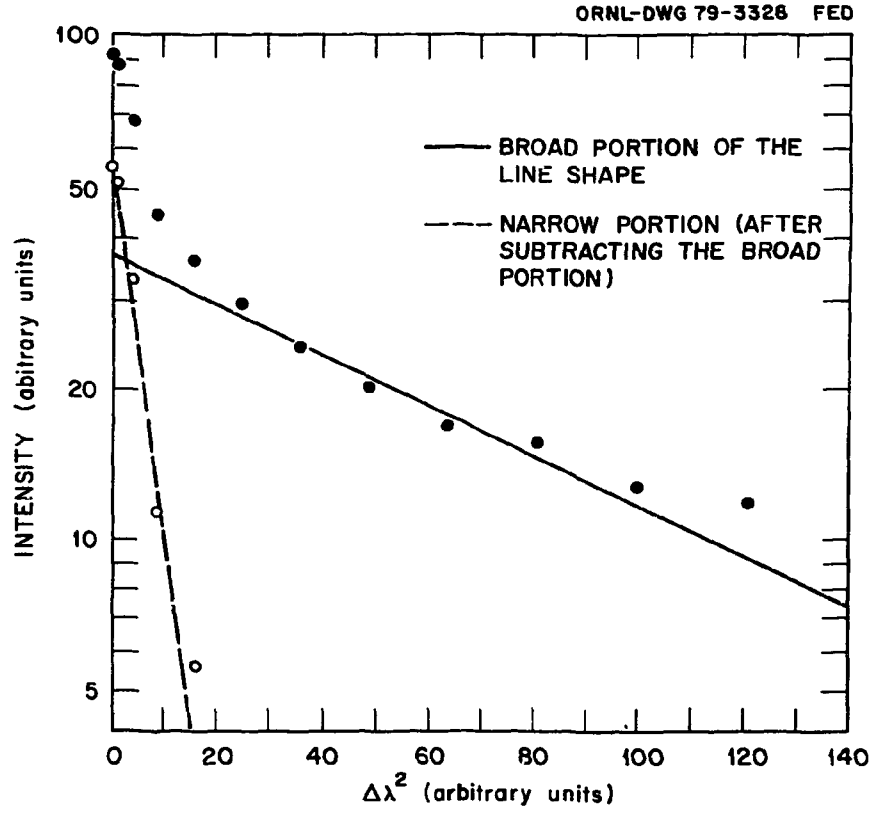

Fig. 9. A semilog plot of the right-hand side of the first peak shown in Fig. 8b. The narrower component is about 0.75 Å wide, and the wider component about 2.5 Å.

off-perpendicular views of the 7-cm beams. The traces start at different times because the FPI sweep was triggered randomly with respect to the beginning of the beam pulse.

Figure 10a shows the effect of varying the viewing angle for a 10-kV, 0.9-A beam. The three traces correspond, from top to bottom, to views at 90° to the beam, at a small downstream angle off 90°, and at a larger (about two times) downstream angle off 90°. In the first trace there are only two unshifted peaks, since the beam and beam plasma components overlap. In the second trace the more intense light from the beam is clearly separated from the less intense, unshifted beam plasma component. Further rotation of the mirror leads to greater separation, as seen in the third trace, and would lead finally to overlapping of interference orders in the trace. In the traces of Fig. 10, the beam plasma peak can readily be identified because it is located a fixed distance from the FPI retrace pattern, whereas the beam light peak moves in relation to the retrace pattern as the viewing angle or beam energy is varied.

Figure 10b illustrates the effect of increasing the accelerating voltage for 1-A beams from 10, to 15, to 20 kV, starting from the top trace, for a fixed viewing angle. Clearly, the relative intensity of the beam plasma light is increasing with the beam energy. This behavior is consistent with observations of unshifted and shifted H_α emission produced in H_2 gas by a proton beam,[10] with specific differences apparently attributable to the different mechanisms and reactions occurring in this experiment. The shift of the full-energy H_α peak to longer wavelengths (to the left in the traces) as the beam velocity increases varies as the square root of the energy.

Finally, Fig. 10c demonstrates the appearance of the full- and fractional-energy beam atoms from a 20-kV beam. The full-energy component is much brighter than the fractional-energy components; the figure shows a distinct bump for the half-energy (E/2) component and a slight enhancement in the signal at the one-third-energy (E/3) component location. The half- and one-third-energy components usually merge, becoming indistinguishable, because of the small difference in speed

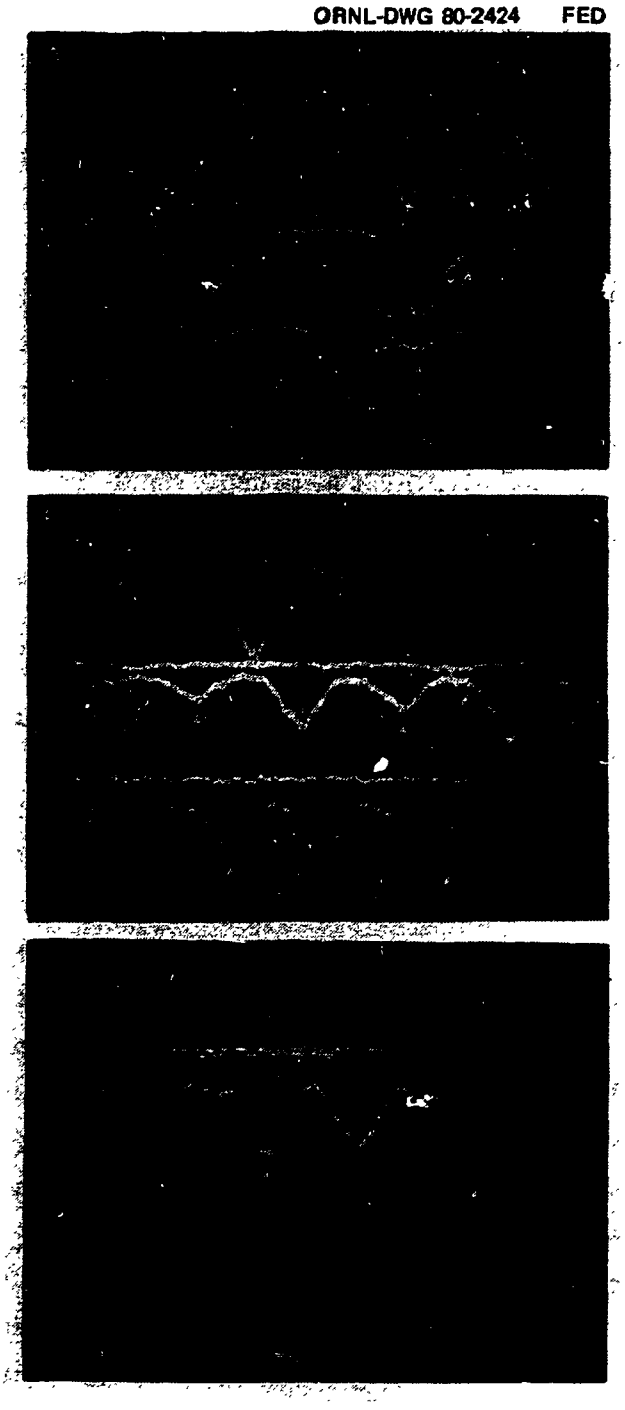

Fig. 10. Data from off-90° views of 7-cm beams, showing (a) the effect of varying the viewing angle, (b) the effect of varying the beam energy, and (c) the occurrence of full- and fractional-energy H_α peaks. In these traces, the full-energy beam light peaks are marked with black arrows inside white borders, the fractional-energy beam light peaks are marked with double circles, and the beam plasma light components are marked with white arrowheads. The wavelength is increasing to the left.

between them. The intensity of the fractional energy components does not appear to agree with estimates of neutral atom fractions based on the charged particle species measurements made on this injector. This may be due to our incomplete knowledge of the excitation processes for H_α in the beam and gas cell and, particularly, of the excitation equilibrium for H (n = 3) at this stage of the beam's passage.

The data from the 7-cm beams yielded good agreement between the accelerator voltage and the displacement of the beam light components with respect to the unshifted beam plasma component. We have observed E/2 and E/3 fractional-energy components with the appropriate wavelength shifts, although the relative intensities of the fractional-energy components do not appear to agree with charged particle measurements. This discrepancy requires further examination. Finally, the divergence evaluated from 90° views at low energies (i.e., below 20 keV, where the beam light intensity is relatively large) is in good agreement with data obtained from target measurements. Off-90° data showed that the width of the full-energy component H_α profile is constant (see, for example, Fig. 10b) within the experimental error over beam energies of 7.5-30 keV. This constant width is lower than that implied by the 90° data, apparently because of a wide fractional-energy component or background (see Appendix C), and implies that the divergence of the full-energy hydrogen atom component is inversely proportional to the beam particle velocity, or the square root of the beam energy. In any case, the 0.3-eV slow dissociation component we have observed in the source experiments places an absolute lower limit on the divergence of a proton beam obtainable from this type of hydrogen plasma discharge. This limit is considerably smaller than the observed divergence.

3.4 HIGH-POWER BEAM EXPERIMENTS

We were able to make a few measurements on a high-power, modified-PLT-type,[11,12] 22-cm-diam neutral beam injector being tested for the ISX tokamak. The beam was viewed across a drift tube, where mostly neutral beam particles and some reionized fast ions are present since the residual ions are deflected away by a bending magnet located between the entrance

to the drift tube and the end of the gas cell. The beam is tailored, however, by the defining aperture and the gas cell. Data were taken with accelerating voltages of 20–45 kV and currents of 18–38 A.

When the beam was viewed exactly at 90° to its axis, the H_α profile showed a slight enhancement on the long-wavelength side, as seen in Fig. 11a. The second trace in Fig. 11a is a repeat of the first, with an interferometer retrace pattern in the middle. The asymmetry was not due to geometric or electrical effects, but apparently to the transverse Doppler effect, which results in a 0.24-Å red shift of the beam light profile from a 35-kV hydrogen beam. In the off-perpendicular case (Fig. 11b and c), the beam plasma light produced a large spike about 0.8 Å wide, and the full-energy beam light yielded a small peak (0.15 to 0.3 the size of the large spike, depending on the accelerating voltage) of roughly the same width. Interpretation of the width of this peak in terms of the beam divergence is difficult because of the smallness of the signal and because the beamlets that compose the beam are aimed at a downstream point (see Appendix B). It is nevertheless interesting to note that there was little, if any, variation in the apparent width (assuming an even background level) of the beam H_α peak (absolute value 1.1 ±0.3 Å) with accelerating voltage or current, just as in the 7-cm beam case. This implies that the beam has a very low divergence. We found very little emission from the fractional-energy components, a finding consistent with the calorimetric particle species analysis (80% full-energy H^0).[12] The background light level was high and appeared to be continuous, as with the 7-cm beams.

Our preliminary data on the high-power beams show that the FPI can be used under these conditions; to obtain quantitative results, however, the sensitivity and noise characteristics of the detector must be improved. It is unlikely that any technique employing broadening of hydrogen lines can be used to view a beam entering an operating tokamak, where the toroidal magnetic field is typically 20 kG or more, because of the smearing of the line profile owing to the local Lorentz electric field produced by the motion of the beam particles across the toroidal field. For H_α light viewed perpendicular to the plane containing the

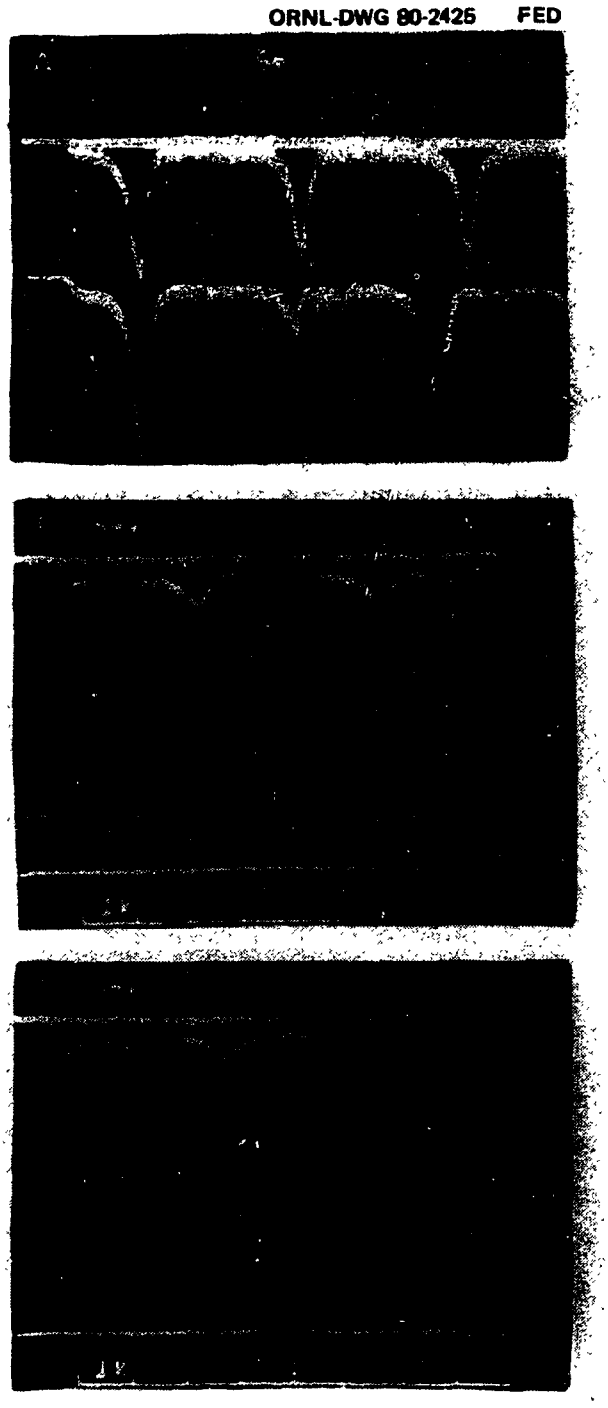

Fig. 11. Data from high-power beams, showing (a) two views across the center of a 35-kV, 35-A beam at 90° to its axis (the wavelength is increasing to the left); (b) a 20-kV, 20-kA beam viewed about 3° downstream from perpendicular; and (c) a 45-kV, 38-A beam viewed from the same angle as in (b). In (b) and (c), the lower trace shows the time variation of the accelerating voltage.

magnetic field and beam velocity vectors, the longitudinal Stark effect would produce a shifting of the line to either side of the center by about $0.01BE^{1/2}$ Å,[13] where E is the beam energy in keV and B is the magnetic field in kG. These wings and the unshifted central Stark component are unpolarized. Thus, for a 40-keV beam and a 30-kG field we obtain a spread of roughly 4 Å. Additional effects owing to Zeeman splitting and plasma Stark broadening, together with the plasma light background, would combine with this effect to destroy the effectiveness of the measurement. The optical method, nevertheless, still offers great promise in a field free situation, such as between tokamak shots, or in a weak field region, such as the upstream drift-duct region.

4. CONCLUSIONS

Though preliminary, these data have provided ample support for the use of the FPI method as an indirect beam diagnostic for divergence, energy, and species measurements. The angular distributions of atoms in beams have been measured approximately, although some improvement in the signal quality is needed. Interpretation of these data in terms of the divergence of a beam comprising a large number of beamlets is rather complicated, but offers a possibility of better understanding of beam particle transport. Doppler shifts of full- and fractional-energy beam atoms varied with the beam energy, as expected. Some inconsistency was noted between the relatively low intensity of the fractional-energy atom contributions to the beam light and the large molecular ion contributions observed in target experiments on the 7-cm beams. Explanation of this discrepancy will require further understanding of the excitation processes in the beam channel. The FPI analysis of H_α light from the ion sources and from the beam-generated background plasmas gave energies of about 0.3 and 2.5 eV, respectively.

ACKNOWLEDGMENTS

We would like to thank R. C. Davis, P. M. Ryan, and C. C. Tsai for help in doing these experiments.

Appendix A

SPECTRAL PROFILE OF BEAM LIGHT VIEWED AT LARGE θ'

As noted in Sect. 2.4, when a Gaussian beam is viewed at angles nearly perpendicular to its axis (i.e., $\theta' \ll 1$), the H_α light from the beam has a Gaussian profile. As θ' increases, however, several effects in addition to the geometric changes described by Eq. (6) will cause distortions in the profile or make it shift.

1. The transverse Doppler shift displaces any beam light profile to the red by an amount $\lambda_o(1 - v_b^2/c^2)^{-1/2}$ regardless of the angle θ' (cf. Fig. 11a).

2. The finite acceptance angle of the FPI optics causes an apparent spread and makes the sampled beam volume asymmetric. This effect occurs for any viewing angle, but it becomes more important when the acceptance angle includes a large volume of the beam outside the plane formed by the beam axis and the viewing direction. Thus, the interpretation of the spectral profile becomes a three-dimensional problem.

3. The spectral profile is distorted by upstream excitation of beam atoms because of the finite mean free path for emission of H_α from excited atoms. This causes both a shift in the peak of the line and a loss of symmetry with a reduction in the profile width from that of Eq. (6).

4. The profile shape will also be distorted because of changes in the background gas pressure and because of beam scrape-off along the beam line. This effect is probably the best reason for viewing at an angle nearly 90° to the beam.

The increasing contribution of these effects as θ' becomes larger would make interpretation of the spectral profile in terms of the beam divergence difficult even in the case of a Gaussian beam.

Appendix B

OPTICS OF MULTIBEAMLET BEAMS

An important consideration in interpreting data from these measurements is the geometry through which the beam passes before it is observed optically. A neutral beam comprises up to a few thousand beamlets focussed, theoretically, to a common point, typically at the end of a beam line. Each beamlet can be regarded as proceeding from a point source and as having an approximately Gaussian angular divergence.[14]

Our analysis in Sect. 2.4 is based on the assumption that the beam is viewed in its "far-field" region (by analogy with the far-field region of wave optics); that is, the beam particles move as if they all originated at a point source far upstream of the observation point and do not interact with one another or with any other object. This assumption is probably true of the individual neutralized beamlets, but the combined profile is a result of the single-beamlet divergence, beamlet focussing, and reactions with background gas molecules. Focussing of the beamlets to a point downstream of the ion source increases the apparent line width of the beam light above the width expected from a single beamlet — or from a beam made up of unfocussed, parallel beamlets — by an amount that is on the order of the angle subtended by the accelerator electrode at the "focal point." Thus, although beamlet focussing reduces the calorimetrically determined beam diameter at the focal point, it increases the apparent beam divergence observed spectroscopically.

The spectral profile of light from the beam is invariant with respect to the downstream position provided that the beam particles do not interact and the beam is not perturbed. This characteristic of the spectroscopic technique is fundamentally different from target measurements, such as calorimetry, which yield a different beam intensity profile with varying downstream position.[14] Given the beam diameter at one point and the spectral composition of the beam light, it is theoretically possible to compute the relative power density at any cross section along a symmetric, equilibrated neutral hydrogen beam. If the beam is cut off

by a limiting aperture in its path, a low value of the H_α line width and, thus, of the divergence will be observed. The effect of the aperture skimming will be greatest in the wings of the spectral profile. A true Gaussian beam will "recover" its relative angular intensity distribution far downstream of the limiting aperture.

The FPI technique could be quite useful for determining the angular spread of individual beamlets or groups of beamlets propagating into a large-volume, low-pressure region after neutralization. The distribution of the beam at large angles could be examined to determine whether the profile were Gaussian out to large angles. This optical method should be considerably more sensitive on low-intensity beams than would calorimetric methods.

Appendix C

BACKGROUND LIGHT IN THE FPI DATA

An important feature of the traces taken at an off-90° angle, particularly at higher energies, is the failure of the traces to return to the zero level between peaks. The various peaks are spread out, and their overlapping tails, together with the instrument profile, may contribute to the apparent minimum signal. In many cases, however, the apparent baseline (see Figs. 10b, 11b, and 11c) is significantly higher than these contributions imply. This may be due to several factors, including (1) molecular light (H_2 lines) or impurity lines from the beam plasma, (2) unexpectedly broad wings in any of the observed peaks owing to an initially high divergence component in the beam or to scattering of energetic beam particles off background gas particles or the vessel walls, or (3) Doppler-shifted H_α light emitted at various angles from the beam that has been reflected and scattered from the vessel walls. The last effect seems most probable. In this case, the spectrum of the H_α light scattered from the walls would appear as a continuum extending for $v_b/c\ \lambda_o$ wavelength units on either side of the unshifted wavelength λ_o, or about 40 Å on either side of the 6563-Å H_α line for a 20-kV beam.

In the 7-cm beam case, at 90° the FPI viewed a recessed glass window across the chamber from the viewing port, so less light that had been scattered at large angles could enter the optics. Thus, the baseline was indeed much lower in that case. A narrower background continuum may, however, contribute to the apparent width of the wide component in the data of Fig. 8. This could explain the discrepancy between the estimated wide-component FWHM for that case (2.5 Å) and the smaller FWHM of the full-energy beam component in the off-90° data (e.g., Figs. 10b and c, where the FWHM $\lesssim$1.5 Å). The H_α width in the off-90° data has been calculated assuming that the baseline of the H_α spectrum is the continuum level. A similar difference in the background signal level between 90° and off-90° views is evident in the data of Fig. 11, although the broad background continuum is obviously also significant in the 90°

case. A good viewing dump is evidently needed on the surface opposite the viewing port.

REFERENCES

1. C. F. Burrell, W. S. Cooper, W. F. Steele, and R. R. Smith, in *Proc. of Seventh Symp. on Engineering Problems in Fusion Research* (1977), pp. 374-76.
2. M. Ulrickson and J. P. Bussac, in *IEEE Intl. Conf. on Plasma Science (Abstracts)* 1978, p. 18.
3. J. F. Bonnal, G. Bracco, C. Breton, C. DeMichelis, J. Druaux, M. Mattioli, R. Oberson, and J. R. Ramette, *Spectrally Resolved Optical Diagnostics on High Power Neutral Beams*, EUR-CEA-FC-996 (March 1979).
4. M. Born and E. Wolf, *Principles of Optics*, 3rd ed. (Pergamon Press, London, 1965).
5. H. R. Griem, *Plasma Spectroscopy* (McGraw-Hill, New York, 1964).
6. W. L. Stirling, P. M. Ryan, C. C. Tsai, and K. N. Leung, Rev. Sci. Instrum. 50, 102-8 (1979).
7. R. C. Davis, T. C. Jernigan, O. B. Morgan, L. D. Stewart, and W. L. Stirling, Rev. Sci. Instrum. 46, 576 (1975).
8. D. H. McNeill, Bull. Am. Phys. Soc. 24, 971 (1979); also PPPL-1625 (January 1980).
9. J. Kim and R. C. Davis, Appl. Phys. Lett. 30, 130-2 (1977).
10. R. H. Hughes, S. Lin, and L. L. Hatfield, Phys. Rev. 130, 2318-21 (1963).
11. W. L. Stirling, C. C. Tsai, H. H. Haselton, D. E. Schechter, J. H. Whealton, W. K. Dagenhart, R. C. Davis, W. L. Gardner, J. Kim, M. M. Menon, and P. M. Ryan, Rev. Sci. Instrum. 50, 523-27 (1979).
12. J. Kim, W. L. Stirling, M. M. Menon, W. K. Dagenhart, G. C. Barber, R. C. Davis, H. H. Haselton, D. E. Schechter, and C. C. Tsai, *ISX-B Neutral Beam Injector Experiment on a Prototype Beam Line*, Oak Ridge National Laboratory Report ORNL/TM-6896 (September 1979); in press, J. Appl. Phys.
13. H. E. White, *Introduction to Atomic Spectra* (McGraw-Hill, New York, 1934).
14. J. Kim and J. H. Whealton, Nucl. Instrum. Methods 141, 187-91 (1977).

ORNL/TM-7259
Dist. Category UC-20

INTERNAL DISTRIBUTION

1. C. F. Barnett
2. S. C. Bates
3. R. J. Colchin
4. W. K. Dagenhart
5. R. A. Dory
6. P. H. Edmonds
7. W. L. Gardner
8. H. H. Haselton
9. G. R. Haste
10-14. J. Kim
15. J. F. Lyon
16. M. M. Menon
17. P. M. Ryan
18. J. Sheffield
19. W. L. Stirling
20. C. C. Tsai
21-22. Central Research Library
23. Document Reference Section
24-25. Laboratory Records
26. Laboratory Records, ORNL-RC
27. ORNL Patent Office
28-29. Fusion Energy Division Library
30. Fusion Energy Division Communications Center

EXTERNAL DISTRIBUTION

31. C. C. Baker, Argonne National Laboratory, 9700 South Cass Avenue, Argonne, IL 60439
32. J. W. Beal, General Atomic Company, P.O. Box 81608, San Diego, CA 92138
33. K. H. Berkner, Lawrence Berkeley Laboratory, University of California, Berkeley, CA 94720
34. Director, Centre d'Etudes Nucleaires, B.P. No. 6, Fontenay-aux-Roses, France
35. J. F. Clarke, Office of Fusion Energy, Department of Energy, Washington, DC 20545
36. F. Coffman, Office of Fusion Energy, Department of Energy, Washington, DC 20545
37. A. Colleraine, General Atomic Company, P.O. Box 81608, San Diego, CA 92138
38. W. S. Cooper, Lawrence Berkeley Laboratory, University of California, Berkeley, CA 94720
39. H. P. Eubank, Plasma Physics Laboratory, Princeton University, P.O. Box 451, Princeton, NJ 08544
40. T. K. Fowler, Lawrence Livermore Laboratory, University of California, P.O. Box 808, Livermore, CA 94551
41. H. P. Furth, Plasma Physics Laboratory, Princeton University, P.O. Box 451, Princeton, NJ 08544
42. M. Gottlieb, Director, Plasma Physics Laboratory, Princeton University, P.O. Box 451, Princeton, NJ 08544
43. L. R. Grisham, Plasma Physics Laboratory, Princeton University, P.O. Box 451, Princeton, NJ 08544
44. E. B. Hooper, Lawrence Livermore Laboratory, University of California, P.O. Box 808, Livermore, CA 94551

45. R. Huse, Chairman, EPRI Fusion Program Committee, Public Service Electric and Gas Company, 80 Park Place, Newark, NJ 07101
46. E. E. Kintner, Office of Fusion Energy, Department of Energy, Washington, DC 20545
47-51. D. H. McNeill, Plasma Physics Laboratory, Princeton University, P.O. Box 451, Princeton, NJ 08544
52. S. Matsuda, Japan Atomic Energy Research Institute, Tokai, Ibaraki, Japan
53. Library, Max Planck Institut für Plasmaphysik, Garching bei München, FRG
54. G. H. Miley, Nuclear Engineering Program, University of Illinois, Urbana, IL 61801
55. T. Ohkawa, General Atomic Company, P.O. Box 81608, San Diego, CA 92138
56. Library, Plasma Physics Laboratory, Princeton University, P.O. Box 451, Princeton, NJ 08540
57. R. V. Pyle, Lawrence Berkeley Laboratory, University of California, Berkeley, CA 94720
58. G. Schilling, Plasma Physics Laboratory, Princeton University, P.O. Box 451, Princeton, NJ 08544
59. N. N. Semasko, Kurchatov Atomic Energy Institute, Moscow, U.S.S.R.
60. T. Sluyters, Brookhaven National Laboratory, Upton, Long Island, NY 11973
61. E. Speth, Max Planck Institut für Plasmaphysik, Garching bei München, FRG
62. H. S. Staten, Office of Fusion Energy, Department of Energy, Washington, DC 20545
63. L. D. Stewart, Plasma Physics Laboratory, Princeton University, P.O. Box 451, Princeton, NJ 08544
64. D. R. Sweetman, Culham Laboratory, Abingdon, Oxfordshire, United Kingdom
65. K. Takayama, Director, Institute of Plasma Physics, Nagoya University, Nagoya, Japan
66. E. Thompson, Culham Laboratory, Abingdon, Oxfordshire, United Kingdom
67. M. Ulrickson, Plasma Physics Laboratory, Princeton University, Princeton, NJ 08544
68. Office of Assistant Manager, Energy Research and Development, Department of Energy, Oak Ridge Operations, P.O. Box E, Oak Ridge, TN 37830
69-185. Given distribution as shown in TID-4500, Magnetic Fusion Energy (Distribution Category UC-20)

★U.S. GOVERNMENT PRINTING OFFICE: 1980-640-245/090